Properties of the quasi 16 day wave derived from EOS MLS observations

A. J. McDonald,[1] R. E. Hibbins,[2,3] and M. J. Jarvis[2]

[1] This paper describes the use of EOS Microwave Limb Sounder (MLS) data to observe the field of traveling planetary waves with quasi 16 day periods. This study utilizes MLS v2.2 temperature and geopotential data between 1 January 2005 and 31 December 2008 in the range 316 hPa to 0.001 hPa (approximately 8 to 97 km) to examine these waves. Analysis demonstrates that the quasi 16 day wavefield is made up of a number of components with westward and eastward propagating s = 1 and s = 2 waves generally dominant. In the Northern Hemisphere the westward and eastward propagating s = 1 waves have similar magnitudes and are larger than the other modes, while in the Southern Hemisphere, the eastward propagating s = 1 and s = 2 waves are larger than the westward propagating wave modes. All of the modes examined display strong seasonal patterns in the temperature amplitude, significant variability in the wave activity from year to year, and the presence of strong pulse-like patterns in the activity. All of the modes also display large median temperature amplitudes poleward of 40 degrees in both hemispheres. Our analysis also demonstrates that the variability in winter from year to year is larger in the Northern Hemisphere than the Southern Hemisphere. Detailed study also suggests that the exclusion of waves from regions of negative refractive index squared likely forms much of the seasonal pattern observed. Thus, regions of strong westward wind speeds effectively exclude vertically propagating waves as expected from theory. The reflection and absorption of waves associated with critical lines is also likely to explain the frequent occurrence of standing wave patterns in the EOS MLS temperature observations. This study highlights the potential of MLS observations for observing waves from the upper troposphere to the lower mesosphere.

1. Introduction

[2] Global-scale perturbations from the zonally averaged state are a key feature of middle atmosphere dynamics, particularly in winter, and are dominated by quasi-stationary and traveling planetary waves. The large magnitude of these waves means that they can transport significant amounts of energy and momentum both vertically and horizontally and these waves are a significant factor in maintaining the zonal mean momentum and temperature budgets of the middle atmosphere [*Holton*, 1980; *Salby*, 1984]. In fact much of the temporal and spatial variability in temperatures, winds and chemical concentrations in the middle atmosphere is due to these wave motions. The role of eastward propagating waves in stratospheric warmings has also been highlighted. For example, studies by *Hartmann et al.* [1984] and *Ushimaru and Tanaka* [1992] have examined the interaction of the stationary wave 1 and the eastward traveling wave 2 in the Southern Hemisphere and the impact on the zonal mean flow. Studies have also shown that during sudden stratospheric warmings the stratosphere-mesosphere system is strongly coupled via planetary wave propagation [*Hoffmann et al.*, 2007]. Traveling waves also play a major role in tracer transport at the equator [*Orsolini et al.*, 1997] and near the polar vortex [*Manney et al.*, 1998]. The planetary wavefield also has a significant impact on the interannual variability of polar ozone depletion [*Huck et al.*, 2005].

[3] Quasi-stationary planetary waves are generally generated by orography and diabatic heating in the troposphere, propagate into middle atmospheric layers and modify the mean flow by depositing heat and momentum. Traveling planetary waves are forced by irregular thermal or mechanical forcing in the lower atmosphere and/or by instabilities in the middle atmosphere. *Salby* [1984] indicates that from solutions of Laplace's tidal equation one can obtain a series of classical normal modes denoted by (s, n − s) for

[1]Department of Physics and Astronomy, University of Canterbury, Christchurch, New Zealand.
[2]British Antarctic Survey, Cambridge, UK.
[3]Now at Department of Physics, Norwegian University of Science and Technology, Trondheim, Norway.

westward propagating Rossby waves, where s is the zonal wavenumber, and n is the meridional index derived from the subscripts of Hough functions. *Salby* [1984] also states that the 16 day wave is identified with the second symmetric wavenumber 1 mode (s, n − s) = (1, 3). However, it should be noted a number of other studies have identified other traveling waves which result from baroclinic or barotropic instabilities.

[4] *Charney and Drazin* [1961] derived a set of equations to explain the vertical propagation of stationary planetary waves which are analogous to that of one-dimensional wave propagation in a medium of variable refractive index. They show that wave propagation is inhibited in regions where the refractive index is imaginary, while in regions where the refractive index is real vertical propagation is permitted. In addition, they demonstrate that an infinite layer in which the refractive index is imaginary will reflect waves totally, while an intermediate negative refractive index squared region between two regions of positive refractive index squared will cause partial reflection. These conclusions are also applicable to traveling waves by accounting for the nonzero intrinsic phase velocities of these waves. The effective refractive index for vertically propagating stationary and traveling planetary waves, in the quasi-geostrophic approximation, depends on the zonal wind [*Charney and Drazin*, 1961; *Smith*, 1983; *Randel*, 1988] with regions of easterly (or westward) flow inhibiting vertical propagation of stationary planetary waves.

[5] Observational studies of these waves can be separated into research which examines the characteristics of these motions using ground-based [*Espy et al.*, 1997; *Mitchell et al.*, 1999; *Espy et al.*, 2005; *Murphy et al.*, 2006; *Hibbins et al.*, 2009] and satellite-based instruments [*Wu et al.*, 1995; *Limpasuvan et al.*, 2005; *Shepherd and Tsuda*, 2008; *Limpasuvan and Wu*, 2009]. A number of studies have also examined these waves in meteorological analyses and re-analyses data sets [*Fedulina et al.*, 2004; *Madden*, 2007]. Combinations of ground-based and satellite-based analyses have also become more common [*Luo et al.*, 2002; *Baumgaertner et al.*, 2008; *Meek and Manson*, 2009].

[6] In this study, we will focus on the properties of the quasi 16 day wave observed by the Microwave Limb Sounding (MLS) instrument onboard the Aura satellite and we will refer to this as the EOS MLS instrument for brevity from this point forward. The utility of EOS MLS for observing traveling and stationary planetary waves has previously been highlighted by a number of studies [*Limpasuvan et al.*, 2005; *von Savigny et al.*, 2007; *Baumgaertner et al.*, 2008; *Limpasuvan and Wu*, 2009]. A key feature of the EOS MLS data is the ability to examine the planetary wavefield from the upper troposphere to the mesosphere and we will highlight this ability in this study.

[7] *Limpasuvan et al.* [2005] and *Limpasuvan and Wu* [2009] both used EOS MLS observations to examine the properties of the quasi 2 day wave. *Limpasuvan et al.* [2005] presented the first observations of the 2 day wave by EOS MLS observations in temperature, water vapor, carbon monoxide, and line of sight wind during December 2004 through March 2005. Their work suggested that the measurements were consistent with the third Rossby-gravity global normal mode. *Limpasuvan and Wu* [2009] detailed

the anomalous behavior of the quasi 2 day wave in the 2006 austral winter.

[8] Work by *von Savigny et al.* [2007] examined temporal variations of the mesopause temperature field with EOS MLS and compared them with noctilucent cloud (NLC) measurements made by the SCIAMACHY instrument. Their study showed that planetary-scale perturbations, in their case the quasi 5 day wave, affect the geographical distribution of the "NLC limb brightness" or the "NLC nadir albedo." In a similar manner, work by *Morris et al.* [2009] displays modulations of Polar Mesosphere Summer Echoes (PMSE) characteristics in VHF radar data associated with planetary-scale waves observed by EOS MLS.

[9] *Baumgaertner et al.* [2008] used a combination of MF radar observations and temperature measurements from the EOS MLS instrument to examine planetary waves with periods between 2 and 4 days in the middle atmosphere over Antarctica. Consideration of the role of vertical shear (baroclinic instabilities) and horizontal shear (barotropic instabilities) of the zonal wind suggests that instabilities are likely to play a role in the forcing of both the 2 and 4 day waves, which are near-resonant modes and thus supported by the atmosphere.

[10] Recent work has also studied the traveling planetary wavefield using observations from the COSMIC satellite [*Shepherd and Tsuda*, 2008; *Alexander and Shepherd*, 2010]. *Shepherd and Tsuda* [2008] focused on the dynamics of the Southern Hemisphere stratosphere in summer at high latitudes and found evidence for eastward traveling waves with wavenumber 1 and 2 with periods of 10, 16, and 23 days.

[11] *Pancheva et al.* [2009] applied a new analysis technique to SABER observations to examine the stationary and traveling planetary wavefield in the Northern Hemisphere winter in 2003/2004. Their spectral analysis indicated that the spectral peaks of the westward traveling waves, particularly those for zonal wavenumber 1, are significantly stronger than the eastward propagating waves in the stratosphere and mesosphere. Work by *Offermann et al.* [2009] has also used SABER data to identify the importance of traveling waves.

[12] This paper describes the use of EOS MLS data to observe the field of traveling planetary waves with quasi 16 day periods and begins by describing the EOS MLS instrument and its measurement capabilities (section 2). Section 3 details the data analysis methodology utilized and also discusses relevant quality control issues and the methodologies used. A description of the climatological features of planetary-scale waves with periods around 16 days is detailed in section 4. In that section we focus on deriving the climatological structure for a range of eastward and westward propagating modes and examine the interannual variability. A discussion of the results previously displayed and initial conclusions are detailed in sections 5 and 6, respectively.

2. Instrument

[13] The Microwave Limb Sounder on the Aura spacecraft observes thermal microwave limb emissions [*Waters et al.*, 2006]. This satellite has a Sun-synchronous orbit with an inclination of 98° (a retrograde orbit) and orbits at 705 km altitude. The satellite orbits the Earth every 100 min and performs 240 scans per orbit which means that the

instrument measures approximately 3500 vertical profiles per day along the suborbital track. EOS MLS measurements cover the geographic latitudes between 82°N to 82°S every orbit and yield concentrations of various chemical constituents as well as temperature and geopotential height. Temperatures between 316 and 0.001 hPa (approximately 8 to 97 km, respectively) are inverted from radiance measurements of O_2 at the 118 GHz and isotopic 234 GHz emission lines. The vertical resolution of the temperature product decreases with altitude, with a value of 4 km at 30 hPa which reduces to 14 km at 0.001 hPa. We utilize version 2.2 temperature and geopotential height data, validation of these data products is described by *Schwartz et al.* [2008]. Temperature and geopotential biases in these observations compared to other instruments are known to exist [*Schwartz et al.*, 2008], but since we measure the perturbations around the mean state these biases should have a minimal impact on most of the results of this study. However, we also use zonal mean geopotential data to derive the geostrophic winds using the method detailed by *Randel* [1987a] and these winds may be affected by these biases. Previous works detailed by *Manney et al.* [2008] and *Manney et al.* [2009] have used the MLS data to derive winds successfully. Their analysis also indicates that flaws in the ECMWF and GEOS-5 reanalyses significantly bias stratopause altitudes during sudden stratospheric warmings and in periods when the stratopause altitude is very high compared to observations and thus our derived winds are likely to be preferable to reanalyses at altitudes above 50 km.

3. Data Analysis

[14] This study uses the least squares method for spectral analysis of space-time series detailed by *Wu et al.* [1995] to examine the quasi 16 day wavefield. Before inputting data into this algorithm the data screening methodologies described by *Livesey et al.* [2007] have been utilized to remove poor quality data. After the screening procedure the mean and standard deviation of the measurements are determined and any observations greater than or less than three standard deviations from the mean are removed to filter out any remaining outliers, this process typically removing 0.25% of the remaining data.

[15] The data is subsetted into 10 degree latitude bins centered from 80°N and 80°S. Each bin has between 180 and 250 points per day before quality control. Within each zonal bin a 48 day sliding window is fit using the procedure detailed by *Wu et al.* [1995]. The time window is then incremented by 1 day and the fit for the next period determined. The choice of the length of time segments is based on the fact that a planetary wave packet is likely to last several periods and the time segment should be sufficient to allow for more than one cycle to be examined. *Fedulina et al.* [2004] concluded that the time segments must be at least 70 days in order to isolate planetary waves with periods between 10 and 20 days. However, work discussed by *Pancheva et al.* [2008] used 45 day time intervals to resolve signatures with periods of 23 days and less and *Shepherd and Tsuda* [2008], using COSMIC data, employed a time segment of 30 days to examine the quasi 16 day wave. We use a period of 48 days which is three times the length of the wave period which we wish to examine. It should be noted

that the selection of this period also defines possible aliasing effects in our analysis. Analysis of wavenumber/frequency spectra (not shown) indicates that the impact of aliasing for the period selected would not cause significant aliasing issues.

[16] *Wu et al.* [1995] show that the length of the period selected also defines the frequency resolution, Δf:

$$\Delta f T = a \qquad (1)$$

where T is the time span selected (48 days in this case) and a is usually taken to be 1.2. Thus, our analysis is sensitive to waves with periods between approximately 13.3 ($1/(f + \Delta f/2)$) and 20 days ($1/(f - \Delta f/2)$) for a bin centered on 16 days.

[17] Because the EOS MLS orbit is Sun-synchronous, the ascending and descending portions of the orbit are stationary with respect to migrating tides. By subtracting the means of the ascending and descending subsets separately the potential impact of aliasing associated with the solar migrating tides are reduced considerably [*Meek and Manson*, 2009].

[18] The noise value associated with the wave amplitude derived from the *Wu et al.* [1995] methodology, which is only used when at least 4000 individual measurements at different time/longitude points are available, will be significantly smaller than the uncertainty on individual points.

[19] We derived a noise level using two methodologies. In the first methodology we selected a set of modes in frequency/wavenumber space that are unlikely to occur and examined the amplitudes derived at these points in frequency/wavenumber space. By analyzing the resultant amplitudes for a whole years worth of results, we can determine noise levels. Analysis suggests that the noise level in temperature amplitude can be very conservatively identified as 0.2 K (the 99th percentile of all amplitude values) and for geopotential height as 12 gpm at 86 km. A second, more conservative methodology, replaced the temperature or geopotential information from EOS MLS observations with values from a gaussian random number distribution with zero mean and a standard deviation associated with the values observed by EOS MLS. The quasi 16 day waves were then fitted to the random data throughout the year including all sampling variations, data gaps and precisions of the original data. The largest amplitude values of the fitted waves (99th percentile from the whole year utilized) were then used to estimate worst case noise levels. Calculations produced a noise level in geopotential height of 19 gpm at 86 km and 4 gpm at 12 km (the 99th percentile values from the whole year were utilized), the variation probably being dominated by the reduction in precision with altitude. The noise level in temperature is 0.3 K at 86 km and 0.15 K at 12 km. We choose to use the noise levels derived by the second methodology in this study as these values are more conservative. Any values derived smaller than these noise levels are either removed from relevant figures or should be ignored.

4. Results

4.1. The Westward Propagating Zonal Wavenumber 1 Quasi 16 Day Wave

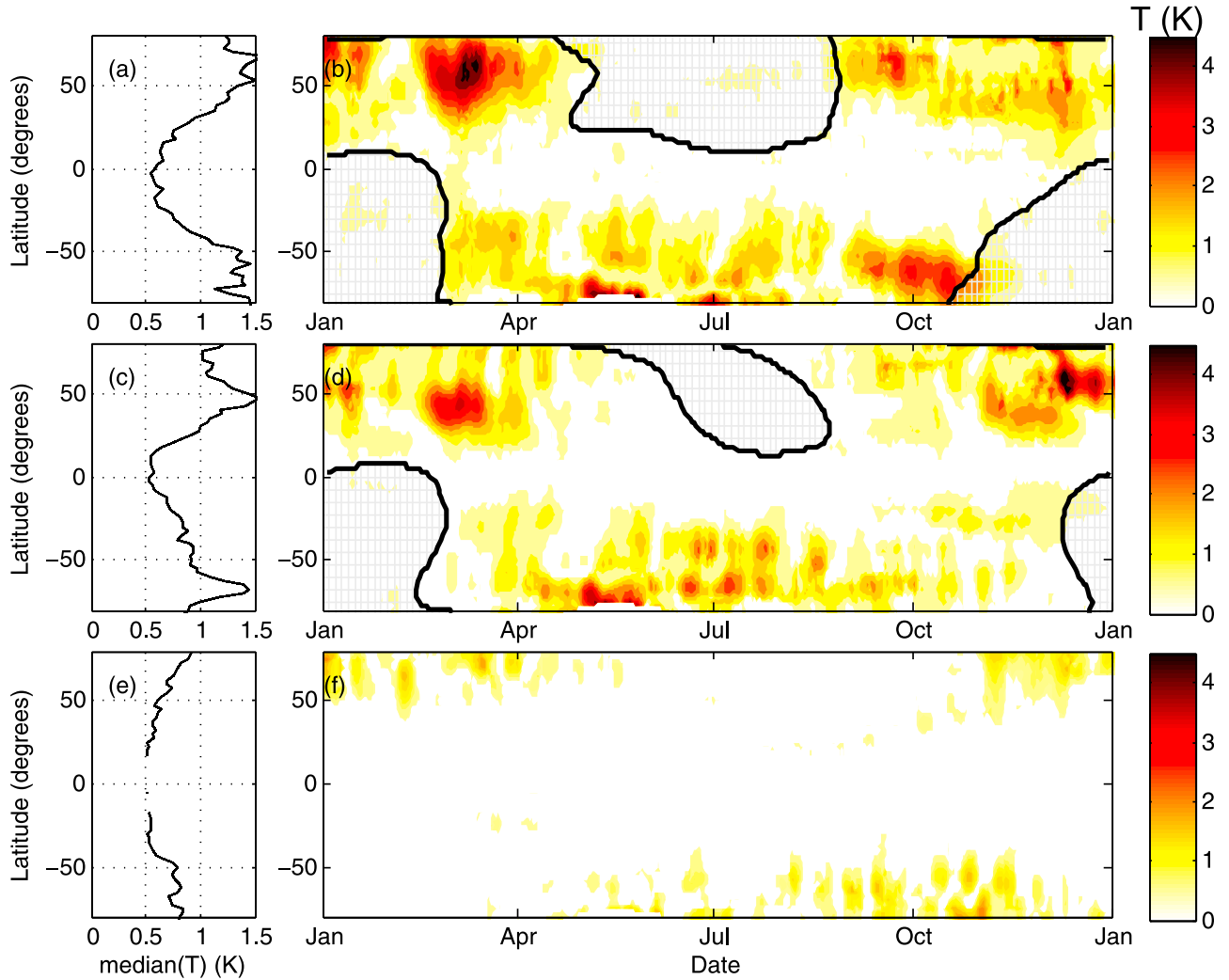[20] Figure 1a shows the median temperature amplitude associated with a 16 day period s = 1 westward propagating

Figure 1. (a, c, e) Median temperature amplitude versus latitude derived for a westward propagating quasi 16 day wave for altitudes of approximately 81, 40, and 19 km, respectively. (b, d, f) Time-latitude contour plot of the temperature amplitude due to the westward propagating 16 day wave derived from EOS MLS observations in 2005 for the three altitudes previously identified.

wave as a function of latitude for an altitude of 81 km, and derived from all the data in 2005. Examination of Figure 1a shows a near symmetric structure around the equator with large median amplitudes poleward of 40 degrees and lower amplitudes toward the equator. Figure 1b displays time-latitude contour plots of the temperature amplitude derived from EOS MLS measurements at 81 km. Figure 1b displays a significant seasonal variation in the planetary wave amplitude. The hatched areas in Figure 1b identify regions in which vertical propagation of the quasi 16 day wave would be excluded by the background zonal winds below this level. Based on simplifications which allow an analytical solution, *Charney and Drazin* [1961] indicated that a planetary wave can only propagate into a region under the following conditions:

$$0 < \overline{u} - c < U_c \qquad (2)$$

where $\overline{u}$ is the zonal mean wind, c is the zonal phase velocity and U_c is the Rossby critical velocity which depends on the

horizontal scale of the wave. Based on equation (2), vertical propagation of waves in the presence of eastward winds is limited by U_c (typically 10's ms^{-1} at midlatitudes). In addition since the zonal phase velocity of a 16 day s = 1 westward propagating wave at 65°S is approximately −12 ms^{-1} waves may only penetrate into somewhat lower-speed westward flows than this value. The intermediate regime identified in equation (2) is associated with real refractive indices (see equations (3) and (4)) and is discussed in more detail in section 5. By identifying geographic regions where the difference between the mean zonal wind and the zonal phase velocity are outside of this range we can identify regions where vertical wave propagation would be excluded. We use the zonal wind climatology of *Hedin et al.* [1996] to derive these exclusion regions in this case. It should be noted that we do not use the geostrophic winds used later in this study to derive these exclusion zones because the geostrophic approximation does not hold near the equator. Figure 1b shows strong seasonal variability in both hemispheres with
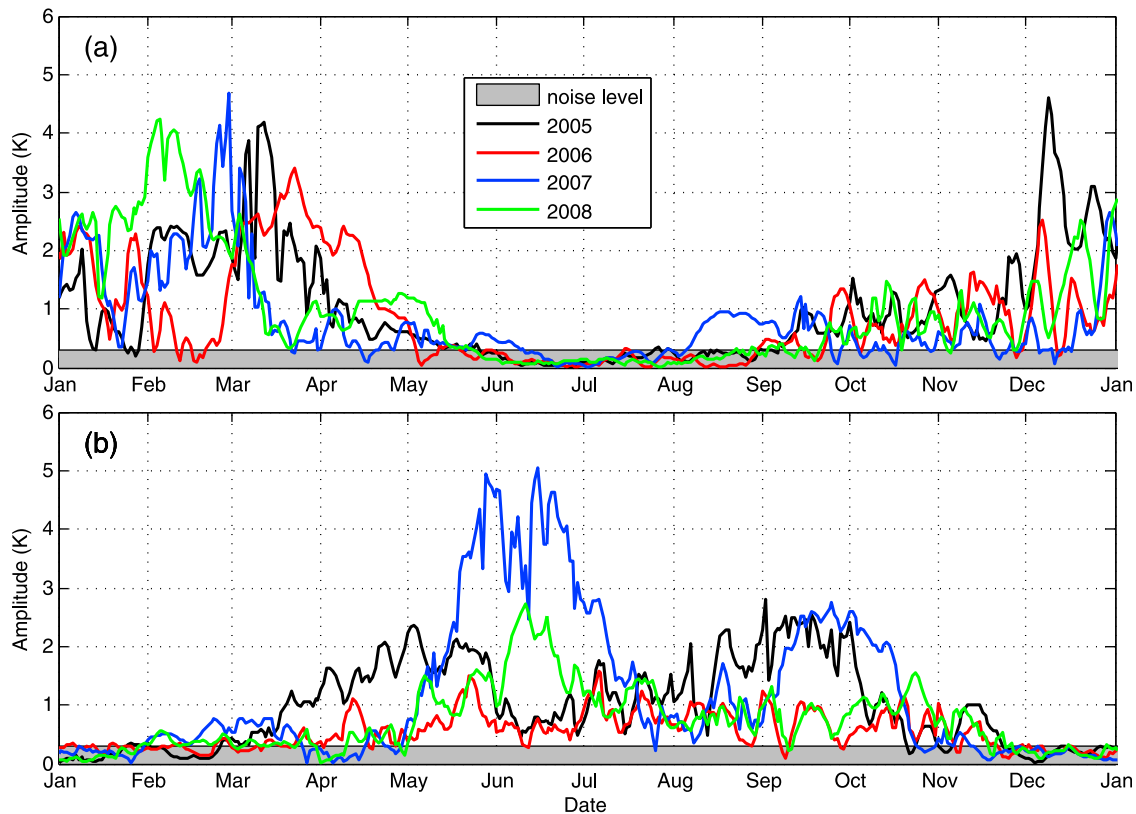
Figure 2. Amplitudes of the temperature perturbations associated with the westward propagating s = 1 quasi 16 day wave at 25 km for latitudes centered around (a) 65°N and (b) 65°S for the years 2005 to 2008 inclusive. The transparent greyed region in the lower part of both Figures 2a and 2b indicates values below a conservative noise floor of 0.3 K.

maximum wave activity being observed in each hemispheres' winter months. The regions where vertical propagation is excluded display significantly less wave activity than other periods and overall, there is a strong correspondence between low wave amplitudes and these exclusion zones at midlatitudes to high latitudes.

[21] Time-latitude contour plots for altitudes of approximately 40 and 19 km for EOS MLS data from 2005 are shown in Figures 1d and 1f, respectively. Examination shows similar patterns to those identified in Figure 1b. However, while the seasonal patterns at the different altitudes are similar, individual wave pulses observed at the different altitudes do not always correspond. This could indicate meridional propagation of the waves. For example, the burst of enhanced wave activity on 1 March centered around 55°N in Figure 1b seems likely to be related to the region of enhanced activity at approximately 40 km at the same time observed at 45°N (see Figure 1d). However, in other cases no correspondence is observed, for example the pulse of activity in October close to 70°S at 81 km does not display a corresponding feature at lower altitudes.

[22] To determine whether these results are typical and to examine the level of interannual variability in the data, Figure 2 displays the temperature amplitudes derived from EOS MLS data at 25 km at 65°N and 65°S for 2005 to 2008 inclusive. Note these latitudes were selected because Figures 1a, 1c, and 1e show they are representative of the region of large temperature amplitudes. Figure 2a shows that

during the period of largest amplitudes which occur between December and March in the Northern Hemisphere there is a significant level of year-to-year variability. The mean amplitudes in February displayed in Figure 2a are 1.35, 1.06, 2.89 and 2.31 K for 2005 to 2008, respectively. Thus, the variation over this 4 year period is close to a factor of 3 in February. Examination of the maximum amplitudes in February (1.92, 2.46, 4.93 and 3.39 K for 2005 to 2008 inclusive) shows variations close to a factor of 2.5 based on this measure. Thus, significant year-to-year variability in the Northern Hemisphere is observed.

[23] Figure 2b also shows a large degree of year-to-year variability in the months with largest amplitude in the Southern Hemisphere, namely May to November at 25 km. For 2005 to 2008 inclusive, the mean amplitudes observed in the Southern Hemisphere in October (see Figure 2b) are 1.02, 0.93, 0.91 and 1.15 K, respectively. Thus, the year-to-year variations observed in the Southern Hemisphere are approximately 25% at this altitude, significantly less than those observed in the Northern Hemisphere. Similar analysis at a range of altitudes between the upper troposphere and the mesosphere suggest that the interannual variations observed at this altitude are in the lower end of the distribution observed. Over all altitudes, the Northern Hemisphere interannual variation over the 4 years examined range from roughly 250% to 750% in February, while the variation ranges from 25% to 300% in October in the Southern Hemisphere. Thus, interannual variability is significantly
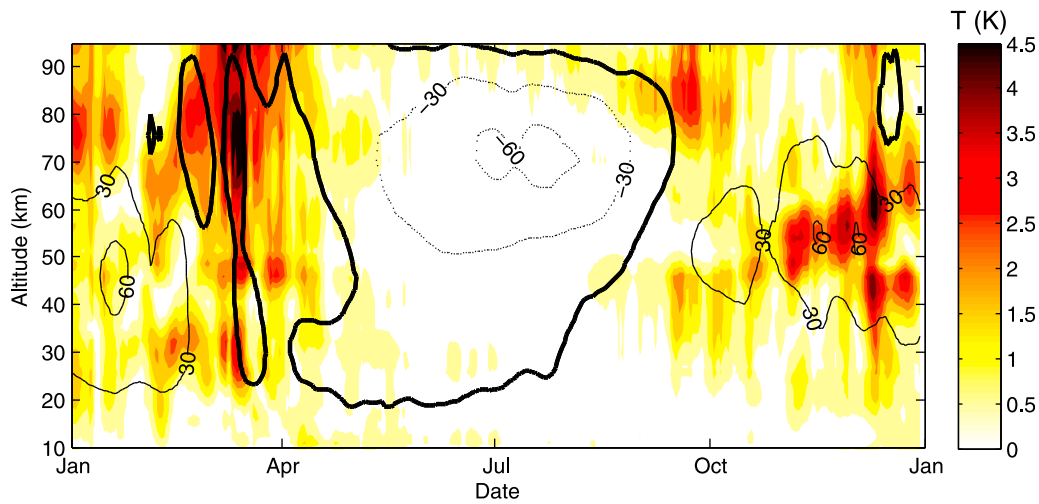
Figure 3. Time-altitude contour plot of the temperature amplitude due to a westward propagating (s = 1) quasi 16 day wave derived from EOS MLS observations for 2005 at 65°N. Contour lines indicate the value of the geostrophic winds derived from MLS observations, the thick line representing the zero wind line.

larger in the Northern Hemisphere in this particular wave component. In addition, amplitudes are generally larger in the Northern Hemisphere than the Southern Hemisphere for this westward propagating wave component.

[24] Figure 3 displays a time-altitude contour plot at 65°N for 2005. Also overlaid on Figure 3 are contours of the zonal geostrophic wind derived from the MLS geopotential data using the analysis detailed by *Randel* [1987a]. The extended altitude range of the EOS MLS temperature measurements allows us to examine planetary waves over an extended region in a manner similar to that previously completed with a combination of meteorological analyses and radar observations by *Lawrence and Jarvis* [2001] and *Lawrence and Jarvis* [2003]. Similar analyses have also been developed using data from the SABER instrument on the TIMED spacecraft by *Palo et al.* [2005] and *Pancheva et al.* [2009] over an altitude range of approximately 20 to 120 km. The most striking feature in Figure 3 is the seasonal variation of wave activity previously observed in Figures 1 and 2. A clear correspondence between variations in temperature amplitude and the zonal mean wind are observed at the seasonal scale. In particular, in the summer when the winds are westward, large amplitude waves are not observed. The temporally variable nature of the zonal winds in the Northern Hemisphere means that some periods of westward winds are observed in winter (see mid-February and early March), but large wave amplitudes still seem to be observed in these regions. This is perhaps associated with the limited region over which the refractive index would be imaginary which would mean that waves would only be partially damped. However, the largest temperature amplitudes are clearly confined to regions where the background zonal winds are predominantly eastward. This concurs with the patterns observed previously in Figure 1 and with theory [*Randel*, 1988, and references therein].

[25] Packet-like structures, potentially associated with the amplification and decay of individual waves as a function of altitude and time, are also observed in Figure 3. For example, waves seem to dissipate well below the maximum altitude observed on 1 December 2005. Clear standing wave patterns characterized by nodes of high- and low-temperature amplitudes are also observed, for instance around 15 March 2005. Similar nodal structures have previously been identified by *Palo et al.* [2005] for a 10 day eastward propagating wave and by *Pancheva et al.* [2009], which compared temperature and geopotential amplitudes and identified a clear relationship between a double peak temperature amplitude structure as a function of altitude and a single peak in the amplitude of the geopotential height anomaly. This pattern which was highlighted by *Salby et al.* [2002] and *Sassi et al.* [2002] results from the hydrostatic relationship between the vertical derivative of the geopotential height anomaly and the temperature anomaly. Figure 4 displays a time-altitude contour plot at 65°N for 2005 for the geopotential amplitude. Comparison of Figures 3 and 4 shows a number of periods where a double peaked temperature structure and a single peak in the geopotential amplitude occur. For example, variations as a function of altitude around 10 December with an upper temperature maxima at 65 km are very clear and a corresponding geopotential maxima around 50 km is also observed. It should be noted that the hydrostatic relationship between temperature and height (and therefore geopotential height) is built into the MLS retrieval.

[26] Some of the variations in wave amplitude observed indicate the possibility of interaction with the mean flow or wave-wave interactions. For example, variations in the background wind as a function of time in the Northern Hemisphere sometimes seem to be related to regions where the wave activity varies significantly, given the role of planetary wave breaking in sudden stratospheric warmings this relationship might be expected.

[27] To determine whether the patterns observed in Figure 3 occur in both hemispheres and also to examine interannual variability, Figure 5 displays a time-altitude contour plot at 65°S for January 2005 to December 2008. Overlaid on Figure 5 are contours of the zonal geostrophic wind derived from the MLS geopotential data. A clear relationship
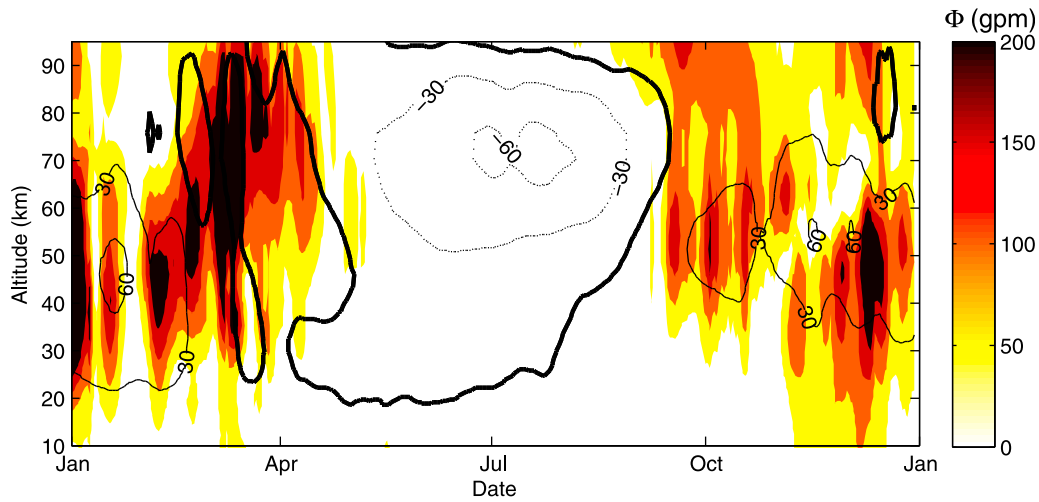
Figure 4. Time-altitude contour plot of the geopotential amplitude due to a westward propagating (s = 1) quasi 16 day wave derived from EOS MLS observations for 2005 at 65°N. Contour lines indicate the value of the geostrophic winds derived from MLS observations, the thick line representing the zero wind line.

between temperature amplitude and zonal mean wind at the seasonal scale is again observed. However, these patterns are more apparent than those in Figure 3, in particular the large temperature amplitudes are confined to regions where the background zonal wind is eastward as expected theoretically. This clarity is probably due to the strength and uniformity of the zonal winds in the Southern Hemisphere winter relative to those in the Northern Hemisphere.

[28] The exclusion of waves from regions of westward flow is particularly clear at altitudes below 30 km where large wave amplitudes are only observed in regions of eastward flow in October to January (see Figure 5). This produces triangular (or wedge) structures in the wave amplitude in which the triangle's diagonal is strongly related to the transition region between westward and eastward winds in each year. This triangular structure is clear below the critical line (at −12 ms^{-1} for a westward propagating s = 1 quasi 16 day wave at this latitude) in October 2005 to January 2006 in Figure 5. Similar patterns have been discussed in relation to COSMIC data by *Alexander and Shepherd* [2010]. Figure 5 also displays regions at higher altitudes, above 80 km in January 2007 and 2008, where planetary wave temperature
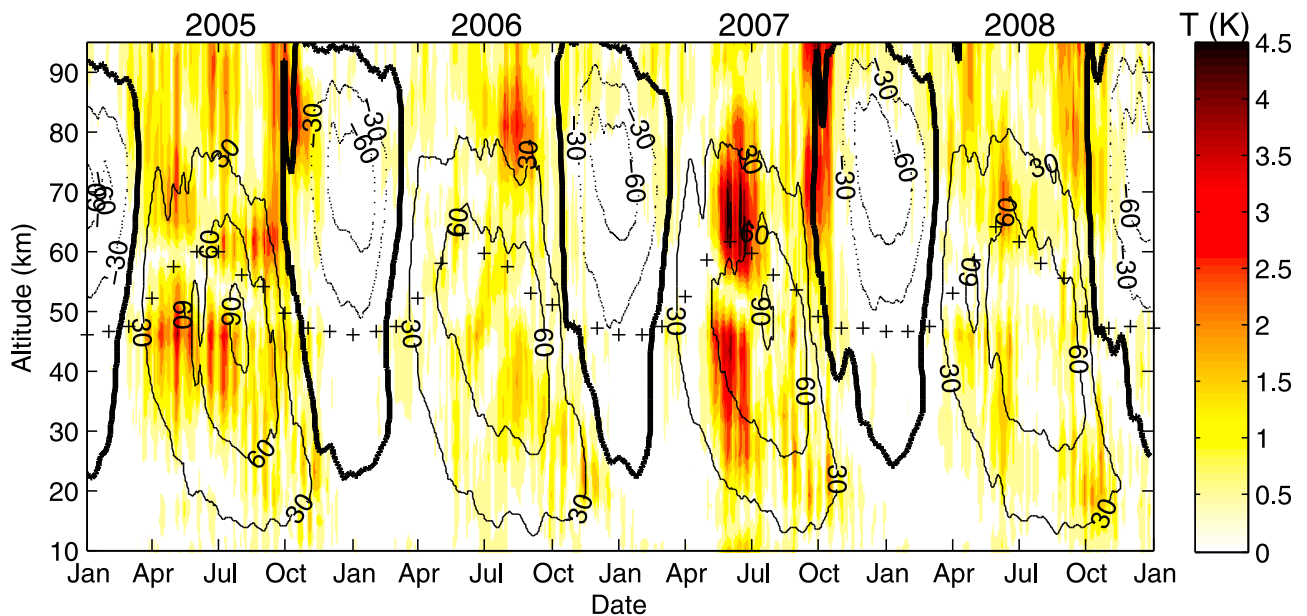

Figure 5. As in Figure 3 but for 65°S and for the period 2005 to 2008. Contour lines indicate the value of the geostrophic winds derived from MLS observations, the thick line representing the zero wind line. The approximate position of the stratopause, derived using a 4th-order polynomial fit to the temperature profile to improve vertical resolution, on the first of each month is also displayed by the crosses.
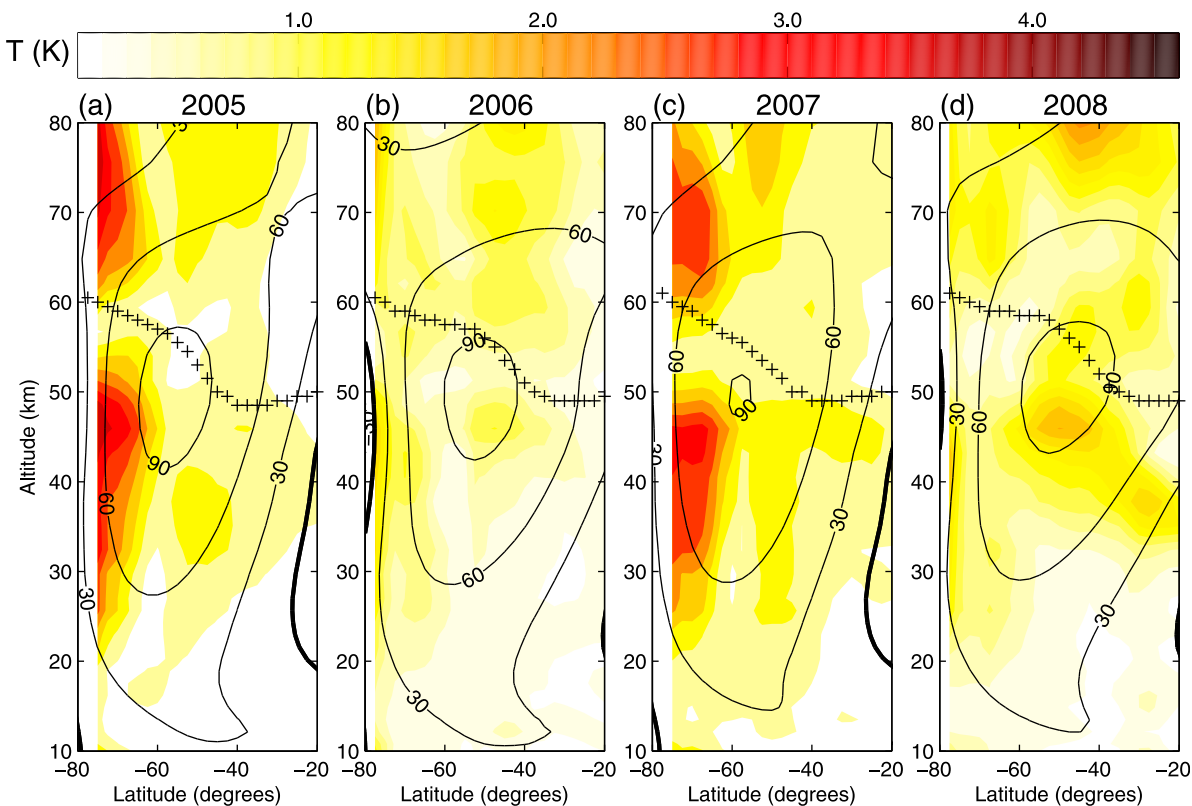
Figure 6. Latitude-altitude contour plots for the Southern Hemisphere in May for (a) 2005, (b) 2006, (c) 2007, and (d) 2008. Contour lines indicate the value of the geostrophic winds derived from MLS observations, the thick line representing the zero wind line. The approximate position of the stratopause, derived using a 4th-order polynomial fit to the temperature profile to improve vertical resolution, on the first of each month is also displayed by the crosses.

amplitudes well above the 0.3 K noise level are observed in regions of eastward winds. These waves are largest in the 2006/2007 and 2007/2008 Southern Hemisphere summer and smaller in the 2005/2006 summer.

[29] Inspection of the wave amplitude contours in Figure 5 shows burst-like behavior similar to that in Figure 3, the signal being particularly clear in June 2007. Given the relationship between the geopotential and temperature amplitudes detailed previously, these minima in the temperature amplitude are likely related to regions where the geopotential amplitude is a maxima. Interestingly, these minima in the planetary wave temperature amplitude seem to coincide with altitudes a few kilometers below the stratopause level, identified by crosses in Figure 5, and in regions of high negative wind shear in May to November. These changes cause variations in the refractive index which could lead to meridional propagation of waves. Therefore, to examine whether these patterns are partially related to meridional propagation, Figure 6 displays latitude-altitude contour plots of the average temperature amplitude observed in May for the Southern Hemisphere for 4 years. Figure 6 also displays mean zonal wind contours and the approximate stratopause altitude derived from the May average zonal mean temperature (crosses). Figure 6 shows that the variations in the amplitude near the stratopause are observed in every year, but are particularly clear at high latitudes in 2005 and 2007.

Figure 6 highlights that the patterns observed in Figure 5 are not generally associated with meridional movement of the waves. Thus, it seems that these variations are representative of changes in the magnitude of the wavefield close to the stratopause. Given that these variations occur in regions where the vertical derivative of the zonal wind and temperature are varying significantly this could be associated with variations in the refractive index of the atmosphere in this region, we explore this possibility in section 5.

4.2. Other Wave Modes

[30] So far this study has focused on the s = 1 westward propagating component of the quasi 16 day planetary wavefield. However, recent studies have demonstrated that the planetary wavefield consists of a large number of components [*Palo et al.*, 2005; *Shepherd and Tsuda*, 2008; *Pancheva et al.*, 2009] and thus we examine other components in the remainder of this section. Figure 7a displays the median temperature amplitude associated with a 16 day period s = 1 eastward propagating wave as a function of latitude for an altitude of 81 km and derived from all the data in 2005. Figure 7a shows a roughly symmetrical structure around the equator with larger values of the median wave amplitude poleward of 40 degrees in both hemispheres. This pattern is similar to that previously shown in Figure 1a except that a peak in wave activity is also observed
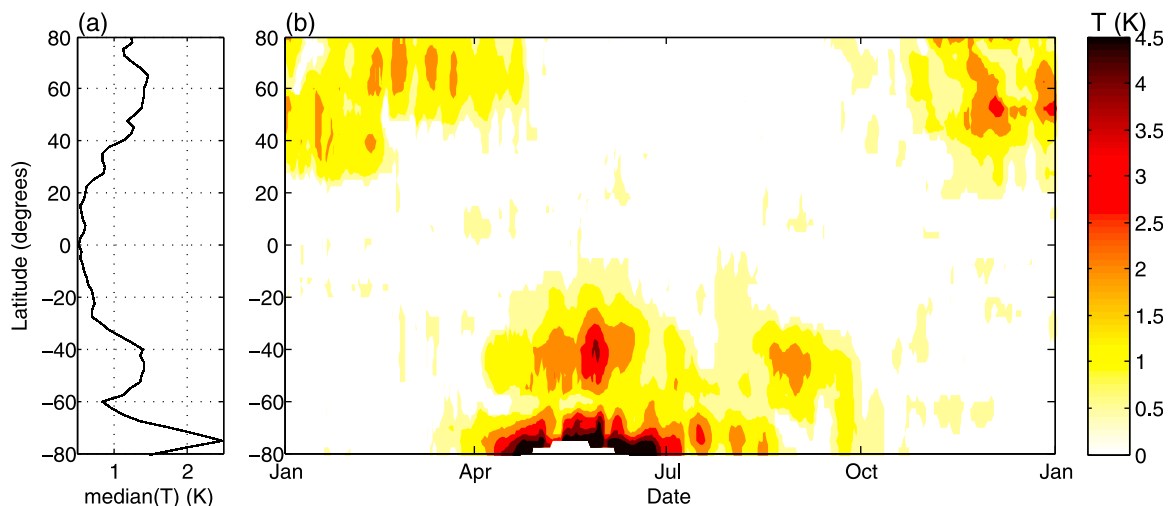
Figure 7. Time-latitude contour plot of the temperature amplitude due to the eastward propagating 16 day wave derived from EOS MLS observations at approximately 81 km.

at high latitudes in the Southern Hemisphere. A time-latitude contour plot of the temperature amplitude derived for observations made in 2005 is shown in Figure 7b and shows strong seasonal variability with maximum wave activity in the winter hemisphere. In this case, the amplitudes of the eastward propagating waves are in general smaller than the westward propagating wave amplitudes when Figures 1b and 7b are compared. In the case of eastward traveling waves, we choose not to display simple exclusion zones based on the waves' phase velocity. We make this choice because the phase velocity for a s = 1 eastward propagating 16 day wave would be +12 ms^{-1}. Thus, given the seasonal pattern of winds we might expect wave propagation to be excluded throughout the year since the wind speeds between the tropospheric and stratospheric jets often fall below this value, though unfortunately we do not have MLS measurements over this entire region. However, this simple analysis would be flawed in this case because the altitude region associated with negative values of the refractive index squared would be very limited vertically in the winter (less than one scale height) and thus we would expect only partial reflection to occur based on the theory by *Charney and Drazin* [1961]. In the case of westward propagating waves this simplification is not an issue because the exclusion zones represent altitude ranges of many scale heights and are therefore a good approximation based on linear theory. However, more detailed analysis discussed in section 5 shows that regions where vertically extended regions of imaginary refractive index occur in summer for eastward propagating waves and thus this pattern probably explains the seasonal pattern of wave activity observed.

[31] Figure 8a shows time series from 1 January 2005 to 31 December 2008 at three different altitudes (25, 40 and 70 km) for the eastward propagating (s = 1) quasi 16 day wave in the Northern Hemisphere. Examination of Figure 8a shows a strong seasonal pattern with maxima in winter and minima in summer at each altitude. Comparison of the amplitude patterns from year to year shows strong interannual variability which is particularly clear when the maximum amplitudes at 40 km in January and February 2008

are compared with amplitudes in the same month in other years. Examination of the relationship between the amplitudes derived at different heights shows a strong positive correlation in general, but specific periods and events show less correspondence. For example, the reduction in wave amplitude at 25 km compared to increases at higher altitudes observed in January to February 2006 is extremely clear. *Manney et al.* [2008] indicated that this period was associated with a major stratospheric warming which occurred on 21 January 2006. Note that all amplitudes increase in the period between February and April 2006 with this behavior being observed at the highest altitudes first. A number of studies have shown that mesospheric wind reversals precede those in the stratosphere which might explain this pattern [see *Hoffmann et al.*, 2007, and references therein] if the waves propagated into this region meridionally.

[32] The Southern Hemisphere pattern is displayed in Figure 8b for data from 1 January 2005 to 31 December 2008 for the s = 1 (eastward propagating) quasi 16 day wave and similar characteristics to those observed in the Northern Hemisphere can be identified. In particular, comparison of Figures 8a and 8b shows similar levels of variability in a relative sense for both hemispheres. Examination of the altitudes between the upper troposphere and the mesosphere indicates that the interannual variability in the Northern Hemisphere has a range of approximately 150% to 850% based on the mean amplitudes for February. In the Southern Hemisphere the interannual variation is more consistent as a function of altitude and has values between 150% and 250% derived from the October mean amplitudes. Comparison of the relative magnitude of the eastward propagating wave at 25 km with the westward propagating wave amplitudes displayed in Figure 2 shows that eastward propagating waves are generally larger. Over the entire altitude range observed by EOS MLS (not shown) the eastward propagating waves are approximately 75% larger than the westward propagating waves based on the October mean values. The dominance of eastward propagating waves indicated by *Alexander and Shepherd* [2010] is therefore at least partially confirmed by these observations.
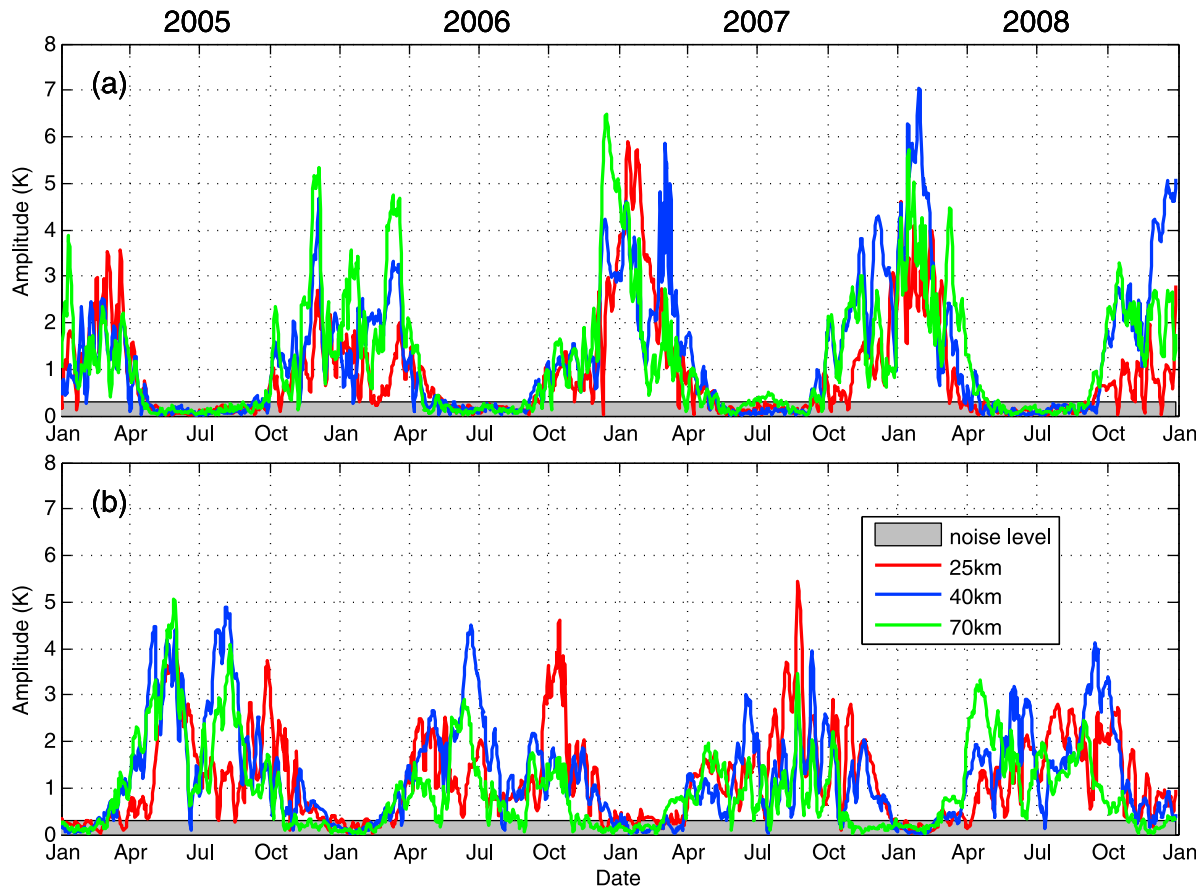
Figure 8. Amplitudes of the temperature perturbations associated with the eastward propagating s = 1 wave at three different altitudes for the period 2005 to 2008 at latitudes centered around (a) 65°N and (b) 65°S.

[33] Previous work by *Shepherd and Tsuda* [2008] and *Alexander and Shepherd* [2010] suggest that long-period wave modes with wavenumbers other than s = 1 also make an important contribution to the wavefield. Figure 9 displays the amplitude of temperature perturbations at two latitudes for the quasi 16 day eastward and westward propagating waves with zonal wavenumbers between 1 and 3 observed at approximately 40 km during 2005. Examination of Figure 9a shows that the wavefield is usually made up of a number of modes and that they all have a similar seasonal pattern, but s = 1 eastward or westward propagating waves tend to be larger than s = 2 and s = 3 modes in the Northern Hemisphere. The eastward propagating wave modes are generally larger than the westward propagating wavefield in the Southern Hemisphere in Figure 9. Inspection of the eastward and westward s = 2 and s = 3 waves show similar seasonal patterns of variation to those of the corresponding s = 1 waves, but with smaller amplitudes. The s = 3 components are generally observed to be smaller than all the other wave components, though there are short periods in December in the Northern Hemisphere where the s = 3 mode has the largest amplitude of all modes.

[34] Figure 10a displays time-altitude contour plots of the temperature amplitude of the quasi 16 day s = 1 eastward propagating wave in the Southern Hemisphere, while the eastward and westward s = 2 components are shown in

Figures 10b and 10c, respectively. Each panel in Figure 10 shows a strong seasonal pattern in the temperature amplitude associated with the direction of the zonal wind, significant variability in the wave activity from year to year and the presence of strong pulse-like patterns in the activity. Thus, there are considerable similarities between all the different wave modes. However, while the eastward s = 1 and s = 2 components have a similar or slightly larger magnitude than the westward s = 1 component shown in Figure 5, the westward propagating s = 2 mode has a considerably lower amplitude. Mean values in the Southern Hemisphere in October in the period 2005 to 2008 range from 0.27 to 0.78 K for the westward propagating s = 1, 0.56 to 1.57 K for the eastward s = 1, 0.5 to 0.95 K for the eastward s = 2 and 0.21 to 0.51 K for the westward s = 2 modes. Another point of interest is that the triangular feature previously observed in Figure 5 below 30 km with a diagonal close to the critical line is evident in Figures 10a and 10b. It should be noted that the altitudes at which large amplitudes are observed varies relative to the position of the zero wind line. This will be discussed further in section 5.

[35] The seasonal and altitudinal variation of the three wave components previously shown in Figure 10 for the Southern Hemisphere are displayed for 65°N in Figure 11, and a similar set of patterns is observed. Interestingly, examination of the altitudes below 30 km in the Northern
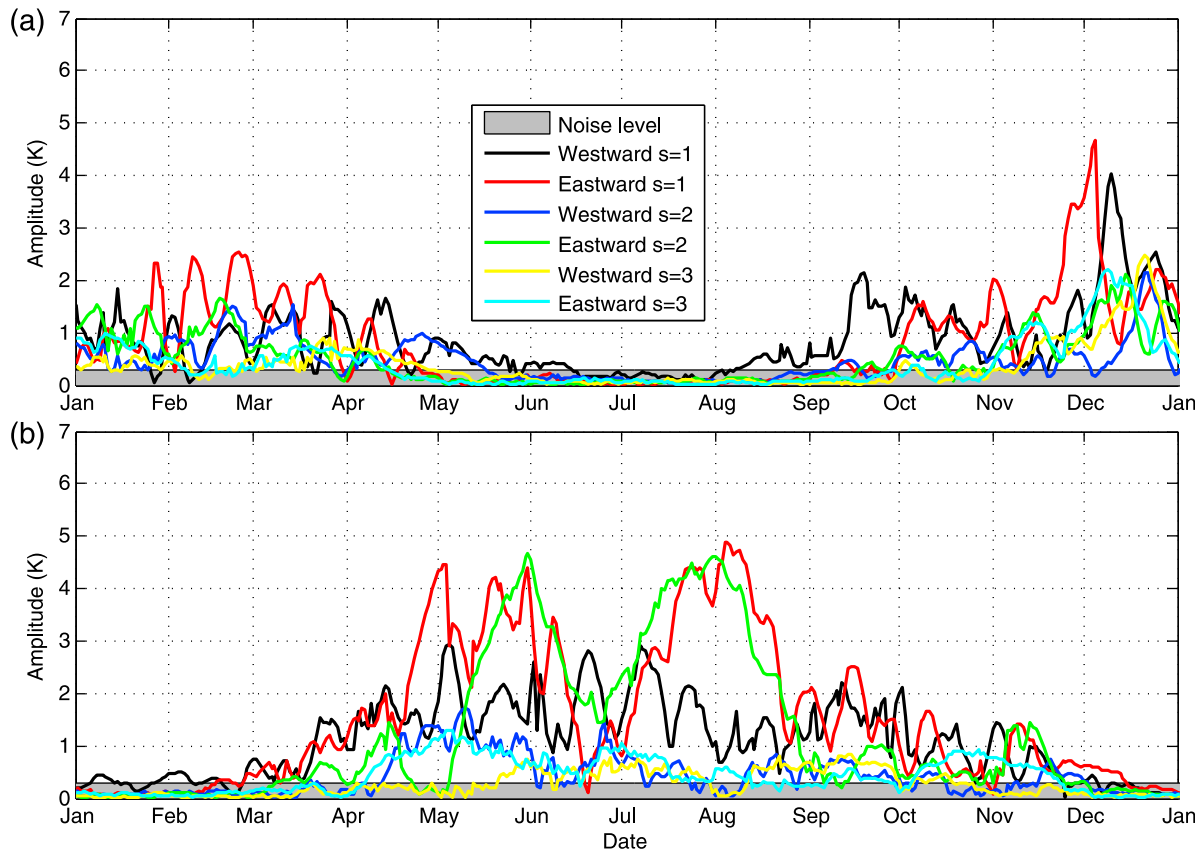
Figure 9. Amplitudes of the temperature perturbations associated with the quasi 16 day eastward and westward propagating s = 1 to s = 3 waves at 40 km for latitudes centered around (a) 65°N and (b) 65°S for 2005.

Hemisphere summer show no sign of planetary wave activity. Figure 3 also shows limited wave activity in this region, suggesting that planetary waves are not precluded from the upper stratosphere in the Northern Hemisphere summer because of the change between eastward and westward winds, but rather because there is little source activity.

5. Discussion

[36] Analysis of Figures 5 and 10 and the mean October amplitudes at a range of altitudes indicates that the eastward propagating wavenumber 1 is generally the largest amplitude mode in the Southern Hemisphere winter, followed by the eastward propagating s = 2 mode. Comparison of Figures 3, 9, and 11 shows that the wavenumber 1 westward and eastward propagating modes have similar magnitudes in the Northern Hemisphere. Amplitudes in February are 1.2 to 2.2 K and 0.48 to 1.08 K for the westward propagating s = 1 and s = 2 modes, respectively, while the range of values for the eastward propagating s = 1 and s = 2 modes are 0.96 to 2.52 K and 0.58 to 1.35 K, respectively.

[37] Previous work detailed by *Meek and Manson* [2009] examined the relative magnitudes of these two waves at 52°N at approximately 92 km in 2005 and found the westward wave was dominant. *Pancheva et al.* [2009] also indicated that for the 2003/2004 Northern Hemisphere

winter that the westward traveling waves, particularly those for zonal wavenumber 1, are significantly stronger than the eastward propagating waves in the stratosphere and mesosphere. This difference between our results and these previous studies seems likely to be explained by the large interannual variability observed in the Northern Hemisphere. This conclusion is potentially supported by work detailed by *Alexander and Shepherd* [2010] which indicated that the eastward propagating waves dominate in both hemispheres in the region between 15 and 40 km based on COSMIC observations.

[38] We now quantify the level of interannual variability in the data. The results presented in section 4 demonstrate a high degree of interannual variability in the wavefield and that the wavefield is often not dominated by a single mode, but made up of a superposition of many waves. The Northern Hemisphere interannual variability shown in Figure 11 displays ranges of approximately 150% to 850% for the eastward propagating s = 1, 300% to 900% for the eastward propagating s = 2 and 150% to 450% for the westward propagating s = 2. The interannual variability in the westward propagating s = 1 mode is 250% to 700% for the February means (also see Figure 2). In the Southern Hemisphere (see Figures 2 and 10), the variation ranges from 125% to 300% in October for the westward propagating s = 1 mode, 150% to 250% for the eastward propagating s = 1 component, 150% to 450% for the
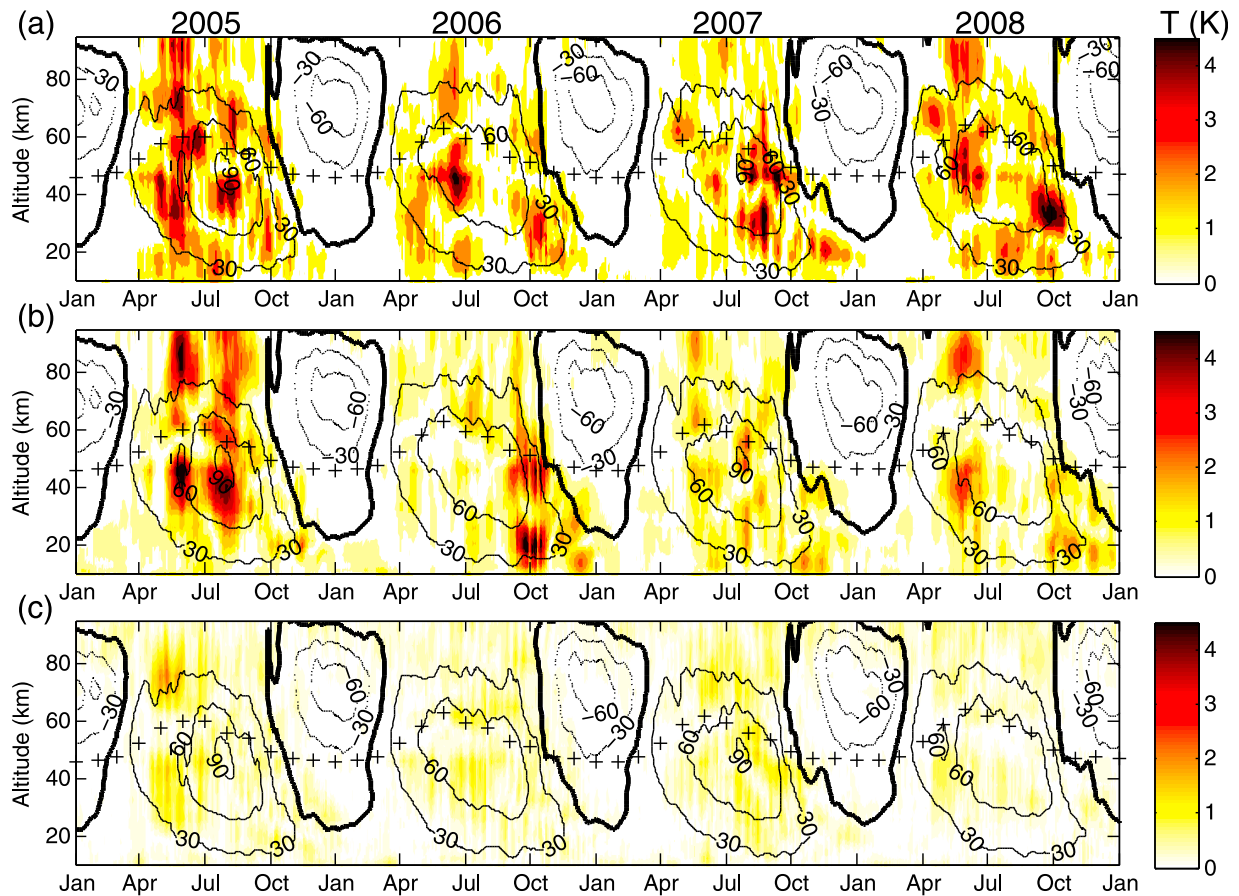
Figure 10. As in Figure 5 but for the eastward propagating wavenumber (a) 1 and (b) 2 and (c) the westward propagating s = 2 components at 65°S.

eastward propagating s = 2 and 150% to 350% for the westward propagating s = 2. The pattern of higher variability in the Northern Hemisphere than the Southern Hemisphere previously identified for the westward propagating s = 1 mode is therefore consistent between the different modes. The largest year-to-year variability is observed in the eastward propagating s = 2 in both hemispheres. The results also suggest that the variability in winter from year to year is larger in the Northern Hemisphere than the Southern Hemisphere.

[39] It has previously been suggested that the interannual variations of the 16 day oscillation observed in the mesosphere in the Northern Hemisphere summer are associated with the equatorial quasi-biennial oscillation (QBO). For example, *Espy et al.* [1997] reported 16 day waves in the summer mesosphere/lower-thermosphere region (80–120 km) at 60°N only during the westward phase of the equatorial QBO in the upper stratosphere. Examination of the 4 years of data used in this study do show some evidence of a westward propagating s = 1 wave in the Southern Hemisphere summer (see Figures 5 and 9), but no clear sign of modulation of this signal by the QBO is observed. This could be a result of the short period examined in this study, and work on this aspect has recently been published [*Day et al.*, 2010].

[40] One interesting feature that has thus far not been explored is the triangular structure below 30 km observed strongly in Figures 5 and 10. To examine this phenomenon more closely, Figures 12a and 12b display the eastward and westward s = 1 temperature amplitudes for the Southern Hemisphere, and Figures 12c and 12d display the eastward and westward components in the Northern Hemisphere for the period and altitude range used by *Alexander and Shepherd* [2010]. Comparison with Figures 9 and 13 in the work of *Alexander and Shepherd* [2010] shows excellent qualitative correspondence, though the low vertical resolution of the MLS observations compared to the COSMIC analysis smears the results. This may result from the different range of wave periods (10–23 days) used by *Alexander and Shepherd* [2010] or from differences in the wave amplitude derivation methodology. Examination of Figures 12a and 12b clearly displays a triangular structure in the Southern Hemisphere for eastward and westward s = 1 waves, respectively. The triangular structure is particularly clear in the eastward s = 1 component (see Figure 12a) with the diagonal below the zero wind line in October to January. In the Northern Hemisphere displayed in Figures 12c and 12d a similar pattern is not observed and no evidence of wave activity above the 0.3 K noise level can be seen. Given that previous studies, such as *Sassi et al.* [2002], have shown that changes in wave amplitude occur approximately two scale heights below the
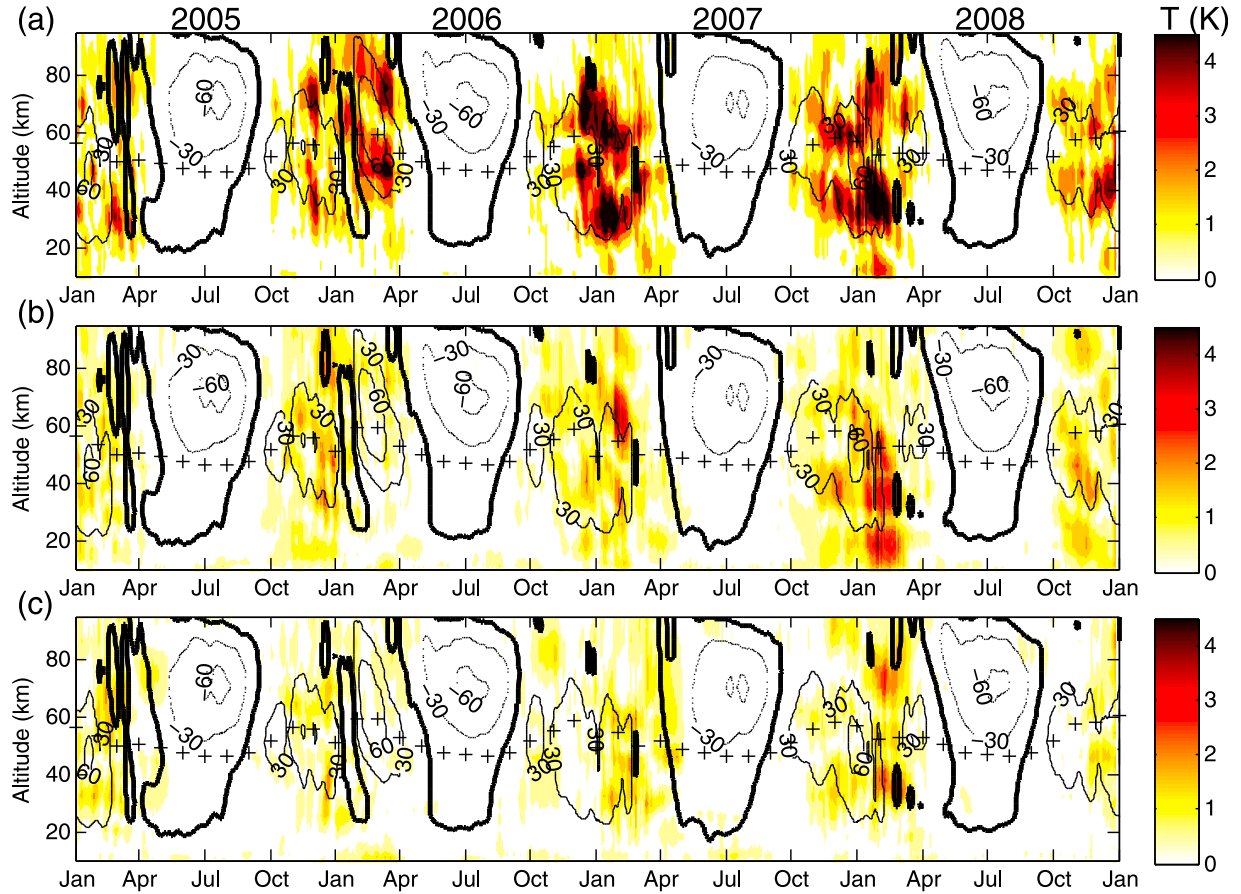
Figure 11. As in Figure 10 but for 65°N.

altitude of the critical line and that the transition from westward to eastward winds is lower in the Northern Hemisphere than the Southern Hemisphere the observed difference between the two hemispheres could simply be associated with removal of the wave below our observational level. However, examination of Figures 12a and 12b shows that the temperature amplitude reduces rapidly near the critical line region and thus suggests that the forcing of these waves in the Northern Hemisphere in this period is not strong or that some process below the level we observe removes these waves.

[41] As previously indicated, theory indicates that there is an effective refractive index for vertically propagating planetary waves, which in the quasi-geostrophic approximation, depends on the zonal wind [*Smith*, 1983, and references therein]. Waves cannot propagate when the refractive index squared is negative, which can occur if the mean wind is easterly, or is westerly but exceeds a wavelength-dependent critical value. The refractive index can be calculated from the gradient in the quasi-geostrophic vorticity which can be written as:

$$\overline{q}_y = \frac{2\Omega}{a}\cos(\phi) - \frac{1}{a^2}\frac{\partial}{\partial\phi}\left[\frac{1}{\cos(\phi)}\frac{\partial}{\partial\phi}(\overline{u}\cos(\phi))\right]$$

$$- (2\Omega\sin(\phi))^2 e^{z/H}\frac{\partial}{\partial z}\left(e^{-z/H}\frac{1}{N^2}\frac{\partial\overline{u}}{\partial z}\right) \quad (3)$$

where Ω and a are the angular velocity and the radius of the Earth, respectively, ϕ is latitude, $\overline{u}$ is the zonal mean wind, z is the altitude above the Earth's surface, H is the scale height and N is the Brunt Väisälä frequency. The quasi-geostrophic refractive index squared, $\overline{Q_{k,c}}$, can then be derived using:

$$\overline{Q_{k,c}} = \left[\frac{\overline{q}_y}{\overline{u}-c} - \frac{k^2}{a^2\cos^2\phi} - \frac{(2\Omega\sin(\phi))^2}{4H^2N^2}\right]/\sin^2\phi \quad (4)$$

where c is the phase velocity of the wave and k is the horizontal wavenumber of the wave. We can use the refractive index squared to diagnose the influence of the zonal mean flow on Rossby wave propagation in the meridional plane more accurately than simply examining the critical line identified by equation (2).

[42] Figure 13 shows a time-altitude contour plot of temperature amplitude for 2005 for eastward and westward $s = 1$ waves with corresponding refractive index squared contour lines overlaid. Examination of Figures 13a and 13b highlights clear regions of prohibited wave propagation in the Southern Hemisphere summer and signs of intermittent regions of prohibited wave propagation in the Southern Hemisphere winter at the highest altitudes observed. This pattern suggests that the wavefield is affected by critical lines close to the stratopause level and this possibility may
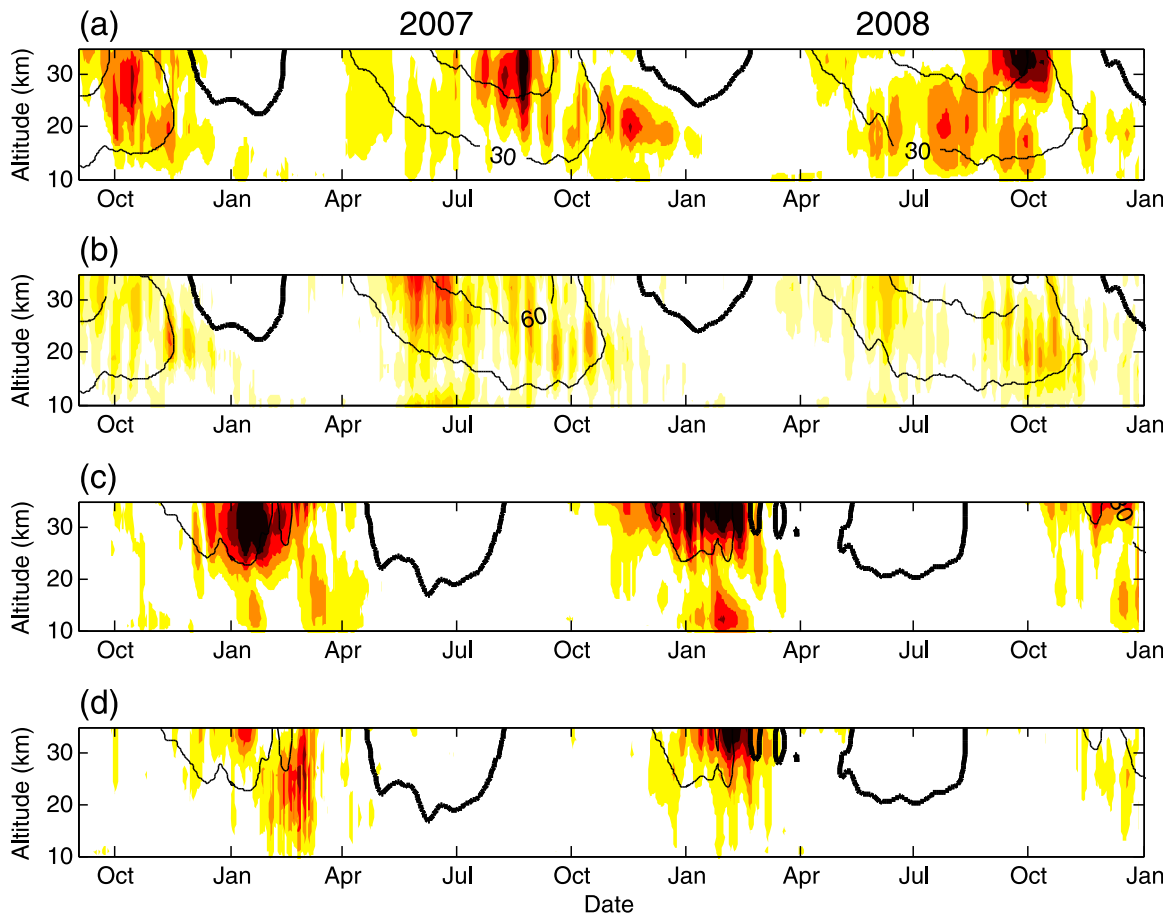
Figure 12. A time-altitude contour plot of the temperature amplitude for a s = 1 (a) eastward and (b) westward propagating quasi 16 day variation in the Southern Hemisphere (65°S) between September 2006 and December 2008. (c) Eastward and (d)westward propagating s = 1 wave in the Northern Hemisphere (65°N). Contour lines indicate the value of the geostrophic winds derived from MLS observations and the values of the colors displayed correspond to the values in the color bar of Figure 11.

explain some of the standing wave features which could result from wave absorption and reflection.

[43] It should be noted that previous works by *Randel* [1987b] and *Manney et al.* [1991] have shown that these waves can propagate vertically from the troposphere to the stratosphere in the Southern Hemisphere winter supporting our viewpoint. However, *Manney et al.* [1991] suggest that in some cases this link cannot be corroborated and that in situ generation from instability mechanisms in the stratosphere may be important in these cases. Work by *Lahoz et al.* [1996] also indicates another alternative view which highlights the potential importance of internal nonlinear vortex interactions. These possibilities only seem to be testable by examining the consistency of the wave phases between altitudes and will be the subject of further studies.

6. Conclusion

[44] The following conclusions can be drawn from this analysis:

[45] 1. The wavefield associated with quasi 16 day periods is often made of a number of eastward and westward propagating wave components, but the s = 1 and s = 2 modes have the largest amplitude. In the Northern Hemisphere the westward and eastward propagating s = 1 wave have the largest temperature amplitude most frequently. While in the Southern Hemisphere, the eastward s = 1 and s = 2 waves are larger than the westward propagating wave modes. The westward propagating s = 2 mode is smaller than the eastward s = 2 mode in both hemispheres.

[46] 2. There are considerable similarities between all the different wave modes. In particular, the same strong seasonal pattern in the temperature amplitude associated with the direction of the zonal wind, significant variability in the wave activity from year to year and the presence of strong pulse-like patterns in the activity is observed in all modes.

[47] 3. The level of interannual variability in both the Northern and Southern hemispheres is very high, reaching factors of two in both the eastward and westward propagating s = 1 and s = 2 modes in both hemispheres. However, the largest year-to-year variability is observed in the eastward propagating s = 2 in both hemispheres. The variability in winter from year to year is larger in the Northern Hemisphere than the Southern Hemisphere.

[48] 4. The exclusion of waves from regions of negative refractive index squared is very clear and is likely to form
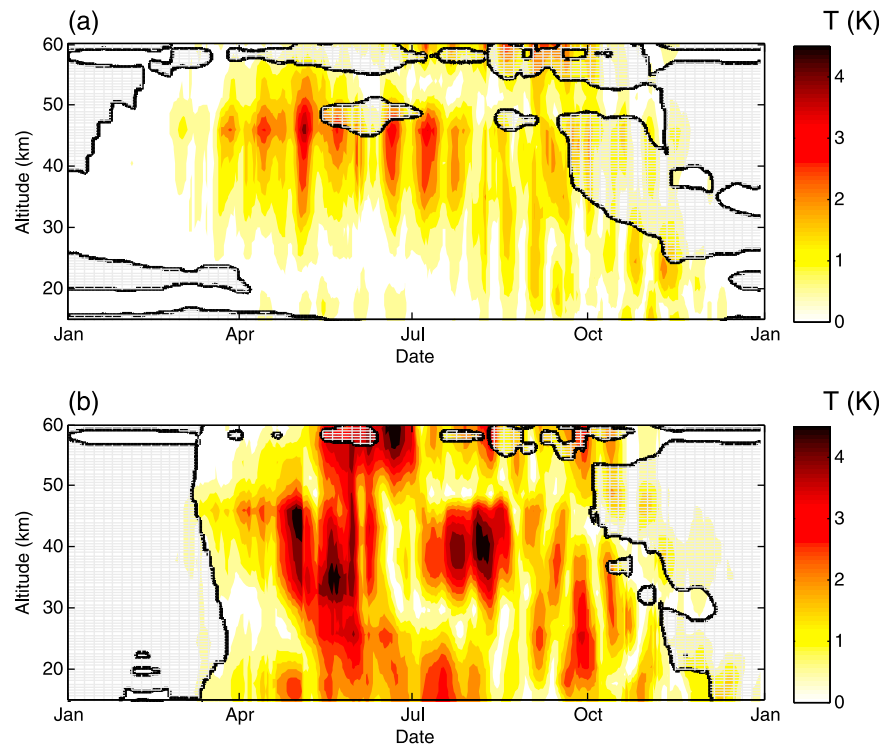
Figure 13. A time-altitude contour plot of the temperature amplitude for a s = 1 (a) eastward and (b) westward propagating quasi 16 day variation in the Southern Hemisphere (65°S) derived from observations in 2005. Contour lines indicate the position of negative values of the refractive index squared.

much of the seasonal pattern observed as might be expected. The reflection and absorption of waves associated with critical lines is also likely to explain the frequent occurrence of standing wave patterns in the EOS MLS temperature observations. However, regions where the vertical propagation of waves from the surface should be excluded display some regions of wave activity above the noise level, primarily in the westward s = 1 mode in the Southern Hemisphere mesosphere and are worthy of further examination.

[49] 5. A brief comparison of the current EOS MLS and COSMIC observations discussed by *Alexander and Shepherd* [2010] demonstrates good qualitative agreement.

[50] Finally, it is clear from this analysis that the MLS observations provide significant potential for quantifying the relationships between the planetary wavefield observed in the stratosphere and mesosphere regions. Given that the quality of reanalyses above the middle stratosphere are likely to be poor [*Manney et al.*, 2009], it also seems likely that deriving information, such as the Eliassen Palm Flux vectors, from the MLS data may be worthy of consideration.

References

Alexander, S. P., and M. G. Shepherd (2010), Planetary wave activity in the polar lower stratosphere, *Atmos. Chem. Phys.*, *10*(2), 707–718.

Baumgaertner, A. J. G., A. J. McDonald, R. E. Hibbins, D. C. Fritts, D. J. Murphy, and R. A. Vincent (2008), Short-period planetary waves in the Antarctic middle atmosphere, *J. Atmos. Sol. Terr. Phys.*, *70*(10), 1336–1350.

Charney, J. G., and P. G. Drazin (1961), Propagation of planetary-scale disturbances from lower into upper atmosphere, *J. Geophys. Res.*, *66*(1), 83–109.

Day, K. A., R. E. Hibbins, and N. J. Mitchell (2010), Aura MLS observations of the westward-propagating s = 1, 16-day planetary wave in the middle atmosphere: Climatology and cross-equatorial propagation, *Atmos. Chem. Phys. Disc.*, *10*, 23,197–23,227.

Espy, P. J., J. Stegman, and G. Witt (1997), Interannual variations of the quasi-16-day oscillation in the polar summer mesospheric temperature, *J. Geophys. Res.*, *102*(D2), 1983–1990.

Espy, P. J., R. E. Hibbins, D. M. Riggin, and D. C. Fritts (2005), Mesospheric planetary waves over Antarctica during 2002, *Geophys. Res. Lett.*, *32*, L21804, doi:10.1029/2005GL023886.

Fedulina, I. N., A. I. Pogoreltsev, and G. Vaughan (2004), Seasonal, interannual and short-term variability of planetary waves in Met Office stratospheric assimilated fields, *Q. J. R. Meteorol. Soc.*, *130*(602), 2445–2458.

Hartmann, D. L., C. R. Mechoso, and K. Yamazaki (1984), Observations of wave mean flow interaction in the Southern Hemisphere, *J. Atmos. Sci.*, *41*(3), 351–362.

Hedin, A. E., et al. (1996), Empirical wind model for the upper, middle and lower atmosphere, *J. Atmos. Terr. Phys.*, *58*(13), 1421–1447.

Hibbins, R. E., M. J. Jarvis, and E. A. K. Ford (2009), Quasi-biennial oscillation influence on long-period planetary waves in the Antarctic upper mesosphere, *J. Geophys. Res.*, *114*, D09109, doi:10.1029/2008JD011174.

Hoffmann, P., W. Singer, D. Keuer, W. K. Hocking, M. Kunzec, and Y. Murayama (2007), Latitudinal and longitudinal variability of mesospheric winds and temperatures during stratospheric warming events, *J. Atmos. Sol. Terr. Phys.*, *69*(17–18), 2355–2366.

Holton, J. R. (1980), Wave-propagation and transport in the middle atmosphere, *Philos. Trans. R. Soc. London Ser. A*, *296*(1418), 73–85.

Huck, P. E., A. J. McDonald, G. E. Bodeker, and H. Struthers (2005), Interannual variability in Antarctic ozone depletion controlled by planetary waves and polar temperature, *Geophys. Res. Lett.*, *32*, L13819, doi:10.1029/2005GL022943.

Lahoz, W. A., et al. (1996), Vortex dynamics and the evolution of water vapour in the stratosphere of the southern Hemisphere, *Q. J. R. Meteorol. Soc.*, *122*(530), 423–450.

Lawrence, A. R., and M. J. Jarvis (2001), Initial comparisons of planetary waves in the stratosphere, mesosphere and ionosphere over Antarctica, *Geophys. Res. Lett.*, *28*(2), 203–206.

Lawrence, A. R., and M. J. Jarvis (2003), Simultaneous observations of planetary waves from 30 to 220 km, *J. Atmos. Sol. Terr. Phys.*, *65*(6), 765–777.

Limpasuvan, V., and D. L. Wu (2009), Anomalous two-day wave behavior during the 2006 austral summer, *Geophys. Res. Lett.*, *36*, L04807, doi:10.1029/2008GL036387.

Limpasuvan, V., D. L. Wu, M. J. Schwartz, J. W. Waters, Q. Wu, and T. L. Killeen (2005), The two-day wave in EOS MLS temperature and wind measurements during 2004–2005 winter, *Geophys. Res. Lett.*, *32*, L17809, doi:10.1029/2005GL023396.

Livesey, N. J., et al. (2007), EOS MLS Version 2.2 Level 2 data quality and description document, technical report, Jet Propul. Lab., Calif. Inst. of Technol., Pasadena, Calif.

Luo, Y., et al. (2002), The 16-day planetary waves: multi-MF radar observations from the Arctic to equator and comparisons with the HRDI measurements and the GSWM modelling results, *Ann. Geophys.*, *20*(5), 691–709.

Madden, R. A. (2007), Large-scale, free Rossby waves in the atmosphere: An update, *Tellus Ser. A*, *59*(5), 571–590.

Manney, G. L., J. D. Farrara, and C. R. Mechoso (1991), The behavior of wave-2 in the southern-Hemisphere stratosphere during late winter and early spring, *J. Atmos. Sci.*, *48*(7), 976–998.

Manney, G. L., Y. J. Orsolini, H. C. Pumphrey, and A. E. Roche (1998), The 4-day wave and transport of UARS tracers in the austral polar vortex, *J. Atmos. Sci.*, *55*(23), 3456–3470.

Manney, G. L., et al. (2008), The evolution of the stratopause during the 2006 major warming: Satellite data and assimilated meteorological analyses, *J. Geophys. Res.*, *113*, D11115, doi:10.1029/2007JD009097.

Manney, G. L., et al. (2009), Satellite observations and modeling of transport in the upper troposphere through the lower mesosphere during the 2006 major stratospheric sudden warming, *Atmos. Chem. Phys.*, *9*(14), 4775–4795.

Meek, C. E., and A. H. Manson (2009), Summer planetary-scale oscillations: Aura MLS temperature compared with ground-based radar wind, *Ann. Geophys.*, *27*(4), 1763–1774.

Mitchell, N. J., H. R. Middleton, A. G. Beard, P. J. S. Williams, and H. G. Muller (1999), The 16-day planetary wave in the mesosphere and lower thermosphere, *Ann. Geophys. Atmos. Hydrosph. Space Sci.*, *17*(11), 1447–1456.

Morris, R. J., A. R. Klekociuk, and D. A. Holdsworth (2009), Low latitude 2-day planetary wave impact on austral polar mesopause temperatures: Revealed by a January diminution in PMSE above Davis, Antarctica, *Geophys. Res. Lett.*, *36*, L11807, doi:10.1029/2009GL037817.

Murphy, D., W. J. R. French, and R. A. Vincent (2006), Long-period planetary waves in the mesosphere and lower thermosphere above Davis, Antarctica, *J. Geophys. Res.*, *111*, D23104, doi:10.1029/2005JD006803.

Offermann, D., et al. (2009), Relative intensities of middle atmosphere waves, *J. Geophys. Res.*, *114*, D06110, doi:10.1029/2008JD010662.

Orsolini, Y. J., V. Limpasuvan, and C. B. Leovy (1997), The tropical stratopause in the UKMO stratospheric analyses: Evidence for a 2-day wave and inertial circulations, *Q. J. R. Meteorol. Soc.*, *123*(542), 1707–1724.

Palo, S. E., J. M. Forbes, X. Zhang, J. M. Russell, C. J. Mertens, M. G. Mlynczak, G. B. Burns, P. J. Espy, and T. D. Kawahara (2005), Planetary wave coupling from the stratosphere to the thermosphere during the 2002 Southern Hemisphere pre-stratwarm period, *Geophys. Res. Lett.*, *32*, L23809, doi:10.1029/2005GL024298.

Pancheva, D., et al. (2008), Planetary waves in coupling the stratosphere and mesosphere during the major stratospheric warming in 2003/2004, *J. Geophys. Res.*, *113*, D12105, doi:10.1029/2007JD009011.

Pancheva, D., R. Mukhtarov, B. Andonov, N. J. Mitchell, and J. M. Forbes (2009), Planetary waves observed by TIMED/SABER in coupling the stratosphere-mesosphere-lower thermosphere during the winter of 2003/2004: Part 2. Altitude and latitude planetary wave structure, *J. Atmos. Sol. Terr. Phys.*, *71*(1), 75–87.

Randel, W. J. (1987a), The evaluation of winds from geopotential height data in the stratosphere, *J. Atmos. Sci.*, *44*(20), 3097–3120.

Randel, W. J. (1987b), A study of planetary-waves in the southern winter troposphere and stratosphere: 1. Wave structure and vertical propagation, *J. Atmos. Sci.*, *44*(6), 917–935.

Randel, W. J. (1988), The seasonal evolution of planetary-waves in the Southern-Hemisphere stratosphere and troposphere, *Q. J. R. Meteorol. Soc.*, *114*(484), 1385–1409.

Salby, M. L. (1984), Survey of planetary-scale traveling waves: The state of theory and observations, *Rev. Geophys.*, *22*(2), 209–236.

Salby, M., F. Sassi, P. Callaghan, D. Wu, P. Keckhut, and A. Hauchecorne (2002), Mesospheric inversions and their relationship to planetary wave structure, *J. Geophys. Res.*, *107*(D4), 4041, doi:10.1029/2001JD000756.

Sassi, F., R. R. Garcia, B. A. Boville, and H. Liu (2002), On temperature inversions and the mesospheric surf zone, *J. Geophys. Res.*, *107*(D19), 4380, doi:10.1029/2001JD001525.

Schwartz, M. J., et al. (2008), Validation of the aura microwave limb sounder temperature and geopotential height measurements, *J. Geophys. Res.*, *113*, D15S11, doi:10.1029/2007JD008783.

Shepherd, M. G., and T. Tsuda (2008), Large-scale planetary disturbances in stratospheric temperature at high-latitudes in the southern summer hemisphere, *Atmos. Chem. Phys.*, *8*(24), 7557–7570.

Smith, A. K. (1983), Stationary waves in the winter stratosphere: Seasonal and interannual variability, *J. Atmos. Sci.*, *40*(1), 245–261.

Ushimaru, S., and H. Tanaka (1992), A numerical study of the interaction between stationary rossby waves and eastward-traveling waves in the Southern-Hemisphere stratosphere, *J. Atmos. Sci.*, *49*(15), 1354–1373.

von Savigny, C., C. Robert, H. Bovensmann, J. P. Burrows, and M. Schwartz (2007), Satellite observations of the quasi 5-day wave in noctilucent clouds and mesopause temperatures, *Geophys. Res. Lett.*, *34*, L24808, doi:10.1029/2007GL030987.

Waters, J. W., et al. (2006), The Earth Observing System Microwave Limb Sounder (EOS MLS) on the Aura satellite, *IEEE Trans. Geosci. Remote Sens.*, *44*(5), 1075–1092.

Wu, D. L., P. B. Hays, and W. R. Skinner (1995), A least-squares method for spectral-analysis of space-time series, *J. Atmos. Sci.*, *52*(20), 3501–3511.

R. E. Hibbins, Department of Physics, NTNU, NO-7491 Trondheim, Norway.

M. J. Jarvis, British Antarctic Survey, Madingley Road, Cambridge CB3 0ET, UK.

A. J. McDonald, Department of Physics and Astronomy, University of Canterbury, Private Bag 4800, Christchurch 8140, New Zealand. (adrian.mcdonald@canterbury.ac.nz)